Triggering of the Pohang, Korea, Earthquake (M_W 5.5) by Enhanced Geothermal System Stimulation

William L. Ellsworth[1], Domenico Giardini, John Townend, Shemin Ge, Toshihiko Shimamoto

[1]Department of Geophysics, Stanford University, 397 Panama Mall, Stanford, California 94035, U.S.A

Abstract

On the afternoon of November 15, 2017, the coastal city of Pohang, Korea, was rocked by a magnitude 5.5 earthquake (M_W, USGS). Questions soon arose about the possible involvement in the earthquake of the Republic of Korea's first Enhanced Geothermal System (EGS) project, as the epicenter of the quake was located near the project's drill site. The Pohang EGS project was intending to create an artificial geothermal reservoir within low-permeability crystalline basement by hydraulically stimulating the rock to form a connected network of fractures between two wells, PX-1 and PX-2 at a depth of approximately 4 km. Forensic examination of the tectonic stress conditions, local geology, well drilling data, the five high-pressure well stimulations undertaken to create the EGS reservoir, and the seismicity induced by injection produced definitive evidence that earthquakes induced by high-pressure injection into the PX-2 well activated a previously unmapped fault that triggered the M_W 5.5 earthquake. Important lessons of a general nature can be learned from the Pohang experience, and can serve to increase the safety of future EGS projects in Korea and elsewhere.

Introduction

The Pohang Earthquake of November 15, 2017

On November 15, 2017, a magnitude (M_W) 5.5 earthquake shook the city of Pohang, Korea (Figure 1). The earthquake caused extensive injuries including dozens of hospitalizations and one fatality, displaced more than 1,700 people into emergency housing and caused more than $75 M (USD) in direct damage to over 57,000 structures and over $300 M (USD) of total economic impact, as estimated by the Bank of Korea. This was the most damaging earthquake to have struck the Korean Peninsula for centuries.

As a consequence of the earthquake, the Pohang Enhanced Geothermal Systems (EGS) project was suspended and the Korean Government commissioned the Geological Society of Korea to produce an evaluation report. An Overseas Research Advisory Committee (ORAC) was formed, consisting of the authors of this paper, with the mandate to elucidate the origin of the Pohang November 15, 2017 mainshock. ORAC worked from March 2018 to March 2019, interacting extensively with Korean colleagues (Korean Government Commission, 2019). The work involved undertaking new analysis and taking into account the results and evidence collected by other groups and researchers working on the earthquake sequence, as well as data made available by the EGS project team (NexGeo and the Korean Institute of Geoscience and Mineral Resources, KIGAM), the Korea Meteorological Administration (KMA), and university researchers not involved in either the official inquiry or the EGS project. This paper presents an abridged version of ORAC's final report, which was delivered on March 20, 2019 as part of the larger findings of the Korean Government Commission (2019) and which is referred to herein as "the ORAC report".

The central question in this investigation was whether the EGS stimulations had triggered this earthquake. One possibility is that the 2017 Pohang earthquake is a natural event unrelated to

EGS activities. Situated on the eastern margin of the Eurasian tectonic plate, the Pohang area and Korea in general exhibit low levels of seismicity in comparison with neighboring Japan and China. However, damaging earthquakes have happened in historical and modern times including the M_L 5.8 (M_W 5.4) Gyeongju event in 2016 (Kim *et al.*, 2018b; Kim *et al.*, 2016; Lee *et al.*, 2018). An alternative view is that the 2017 Pohang earthquake was triggered by the hydraulic stimulations that had taken place at the Pohang EGS site nearby over the previous two years.

The historical and recent occurrence of tectonic earthquakes nearby does not preclude the possibility that the 2017 Pohang earthquake was triggered by EGS activities. While spatial and temporal correlations are the primary basis for linking hydraulic stimulation to earthquakes, they do not necessarily demonstrate causation and in the case of the Pohang earthquake require specific investigation.

Pohang EGS Project Overview

The Pohang EGS Project was intended to demonstrate the potential of geothermal energy production in a ~4 km-deep granitic reservoir overlain by Cretaceous volcanics and sedimentary rocks, Tertiary volcanics and sedimentary rocks, and Quaternary sediments. The Pohang area is one of the highest heat-flow areas in Korea and has been the focus of dedicated geothermal research since 2003 (Lee *et al.*, 2010).

Over the course of approximately four years from 2012 to 2016, two exploratory wells named PX-1 and PX-2 were drilled into the granitic basement to develop the enhanced geothermal system (Figure 1). PX-1 had a designed depth of 4,127 m, but the drill pipe became stuck after crossing 4,000 m and the hole was lost below a depth of 2,485 m. PX-1 was later side-tracked and extended in the WNW direction to a depth of 4,215 m, measured depth (MD) 4,362 m. PX-2 was drilled to a depth of 4,340 m (MD 4,348 m). Note that all depths were measured from the drill rig floor, which is 9 m above the ground surface.

PX-1 and PX-2 are 6 m apart from each other in the north-south direction on the ground surface and are approximately 600 m apart at the bottom. Both wells are cased along their length except for the bottom 313 m in PX-1 and 140 m in PX-2. These bottom intervals are open for fluid injection and flow back.

Five hydraulic stimulations were conducted between January 29, 2016 and September 18, 2017. The first, third, and fifth stimulations were conducted in PX-2 and the second and fourth in PX-1. Each hydraulic stimulation involved multiple cycles of injection of water under high pressure followed by shut-in or flow back. The Pohang earthquake occurred when PX-1 was shut in and PX-2 was open after the fifth stimulation.

Figure 2 shows the injection rates and the net injection volume over the entire period of five stimulations. The volumes of water injected into and flowed back from PX-1 are 5,663 m^3 and 3,968 m^3. The volumes of water injected into and flowed back from PX-2 are 7,135 m^3 and 2,989 m^3. Thus, a net volume of 5,841 m^3 of injected water remained in the subsurface following the stimulations.

In PX-2, the maximum wellhead pressure and injection rate reached 89.20 MPa and 46.83 l/s during the first stimulation. In PX-1, the maximum wellhead pressure and injection rate reached 27.71 MPa and 19.08 l/s during the second stimulation. Injection pressures were higher overall for PX-2 than for PX-1 at similar injection rates. Seismicity accompanied each stimulation and for injection into PX-2 continued for up to several months (Figure 2).

Terminology Used in this Report

Earthquakes can occur as a consequence of a wide variety of industrial activities, including the impoundment of high dams, underground mining, petroleum production and storage, geothermal energy extraction, CO_2 sequestration and wastewater disposal by injection (Ellsworth, 2013; Grigoli *et al.*, 2017). The earthquakes caused by these activities are sometimes referred to as "induced" or "triggered" to identify them as being of anthropogenic origin.

In the scientific literature, "induced" and "triggered" are sometimes used to draw a distinction between earthquakes that primarily release strains created by the industrial process (induced) and earthquakes that primarily release natural tectonic strain (triggered; e.g. McGarr et al., 2002). The term "induced" is also used to refer to all anthropogenic earthquakes, as only human activity can induce earthquakes, while natural earthquakes routinely trigger other earthquakes. Here we adopt the following definitions to describe seismicity in the specific context of activities connected to the Pohang EGS project:

- Induced earthquakes occur within the volume of rock in which pressure or stress changes as a consequence of injection. Their magnitudes are consistent with the spatial dimension of the stimulated volume. They can occur both during injection and after injection ceases. They may release tectonic strains or strains created by injection pressure or volume.

- Triggered earthquakes are runaway ruptures, initiated by anthropogenic forcing that grow in size beyond the bounds of the stimulated region. They release tectonic strain.

Regional Setting

Geology

The Pohang EGS site is located within the Pohang Basin, one of several sedimentary basins that formed in the early Miocene during back-arc extension and opening of the East Sea or Japan Sea (Son *et al.*, 2015). The basin is bordered to the west and south by the NNE-striking

Western Border Fault and the NNW-striking Ulsan Fault System, respectively, which are each composed of strike-slip and normal fault segments that formed during the basin's extensional phase (Cheon *et al.*, 2012; Son *et al.*, 2015). A change in regional tectonics in the late Miocene resulted in broadly ENE–WSW compression across the southeastern Korean Peninsula (Chough *et al.*, 2000; Park *et al.*, 2007) .

Much of the Quaternary faulting recognized in southeastern Korea occurs on subsidiary faults associated with the Yangsan and Ulsan faults (Ree *et al.*, 2003). Those associated with the Yangsan fault tend to be N- or NNE-striking subvertical dextral strike-slip faults, whereas those associated with the Ulsan fault are typically NNE- to NNW-striking reverse faults (Ree *et al.*, 2003).

Korean geologists consider faults that dissect Quaternary formations as active and referred to them as "Quaternary faults". No Quaternary faulting close to the EGS site was recognized prior to the 2017 earthquake, although Quaternary faults had previously been identified within 15 km of the site at outcrops on the Yangsan and Wangsan faults (Ree and Kwon, 2005; Ree *et al.*, 2003).

Seismicity

The historical record of seismicity spans two millennia and reveals that earthquakes have occurred throughout the Korean Peninsula (Lee and Yang, 2006). The attribution of pre-instrumental earthquakes to specific faults is difficult (Houng and Hong, 2013), but the historical catalog indicates the occurrence in southeastern Korea of more than 100 "felt" earthquakes, of which at least 11 produced Modified Mercalli Intensity shaking exceeding VIII [Kim et al., 2018b]. This latter group includes a M~6.7 earthquake in 779 AD and M~6.4 earthquake in 1306 AD. The historical seismicity in southern Korea proves that the major active fault systems identified in the regional geology (such as the Yangsan fault) have been active in historical and recent times (Lee and Yang, 2006).

The most recent large event to occur in southeastern Korea prior to the 2017 earthquake was the M_L 5.8 (M_W 5.4) Gyeongju earthquake of 12 September 2016, which was preceded 48 minutes earlier by a M_L 5.1 foreshock. These events occurred approximately 40 km south of the Pohang EGS site. Aftershock relocations and analysis of the foreshock and mainshock focal mechanisms indicated strike-slip motion on a steeply-east-dipping NNE-striking fault plane at mid-crustal depths of approximately 15 km (Hong *et al.*, 2017; Kim *et al.*, 2018b).

Regional Stress State

The state of contemporary tectonic stress in the Korean Peninsula has been studied by several groups in recent years using a variety of borehole and seismological techniques (Kim *et al.*, 2017; Lee *et al.*, 2017b; Soh *et al.*, 2018). We focus here on those results most pertinent to stress in the vicinity of the Pohang EGS site and at depths comparable to the depth of the 15 November earthquake.

Soh *et al.* (2018) mapped stress parameters throughout the Korean Peninsula using earthquake focal mechanism analysis and documented a strike-slip stress state ($S_v = S_2$), R~0.85 and ENE–WSW S_{Hmax} orientation in southeastern South Korea. Here $R = (S_1 - S_2)/(S_1 - S_3)$, where S_1, S_2, and S_3 are the maximum, intermediate, and minimum principal stress magnitudes, S_v is the vertical stress, and S_{Hmax} is the azimuth of maximum horizontal compressive stress. Analysis of focal mechanisms recorded between 1997 and 2016 within 70 km of the Pohang EGS site yields a strike-slip stress state ($S_v = S_2$), R~0.88, and S_{Hmax} = 074°. The state of stress at shallow depths within ~10 km of the EGS site was investigated using borehole data by Kim *et al.* (2017) and Lee *et al.* (2017a), who derived S_{Hmax} estimates of approximately 130° at depths of ~700 m and inferred the stress state to be strike-slip.

Site Geology and Geophysics

Prior to the drilling of PX-1 and PX-2, an extensive program of geophysical site characterization was undertaken by the Korea Institute of Geoscience and Mineral Resources (KIGAM), as detailed in Chapter 3 of the Korean Government Commission (2019) report on the earthquake. Magnetotelluric measurements revealed west-dipping conductive features beneath the EGS site, which were interpreted as fracture zones and potential geothermal targets (Lee *et al.*, 2015). However, the limited spatial resolution of the models did not enable the presence of a large discrete fault to be determined.

During the drilling of PX-1 and PX-2 the drill cuttings were analyzed at regular depth intervals by on-site geologists who created records of lithologic observations referred to as "mud logs". The stratigraphy consists of Miocene Pohang Basin sediments extending to a depth of ~200 m, overlying Cretaceous sedimentary and volcanic rocks and Paleozoic granodiorite below ~2,350 m. Most drill cuttings are fresh and angular. However, the cuttings from PX-2 in the depth interval from 3,790 to 3,816 m contain a large fraction of friable round-shaped "mud balls". Their microstructure shows a typical fault gouge and breccia structures in which clasts are scattered within a fine-grained and locally foliated matrix. Fragments of cohesive cataclasite were also observed. Cuttings below 3,791 m contain fragments of granite, in contrast with granodiorite mixed with fine-grained igneous rocks at shallower depths. The data illustrated in Figure 3 indicate the presence of a fault gouge and breccia zone several meters in thickness. The major mud loss at a depth of 3,830–3,840 m likely occurred in fractured host rock next to the fault zone.

In August 2018, wireline logging tools were deployed in PX-2 to image the borehole after the earthquake. The logging tools were unable to descend below 3,783 m due to obstruction of the well. This depth nearly coincides with the top of the fault gouge and breccia zone. It is possible that fault movement during the Pohang earthquake caused damage to the borehole at this depth.

State of Stress at the Pohang Drill Site

Dipole sonic logging of the PX-2 borehole acquired in December 2015 revealed the presence of anisotropy features at depths of ~3.4–4.3 km that are interpreted to indicate an axis of maximum horizontal compression (S_{Hmax}) oriented 077±23°. This orientation is consistent with the pre-2017 regional orientation computed from focal mechanisms and is our preferred value in the analysis below.

In the calculations below, we use a stress tensor referred to as the "preferred model" corresponding to a critically-stressed reverse stress state evaluated at 4.2 km ($S_v = S_3 = 106$ MPa), with hydrostatic fluid pressure, $R = 0.90$, and the S_{Hmax} orientation of 077°, determined from the dipole sonic logging undertaken in August 2018. We adopt values for the maximum and minimum horizontal stress magnitudes of $S_{Hmax} = S_1 = 243$ MPa and $S_{hmin} = S_2 = 120$ MPa, respectively. The S_{Hmax} magnitude is computed assuming that the crust is in a state of frictional equilibrium governed by slip on faults with a coefficient of friction of 0.6 (Townend and Zoback, 2000; Zoback, 2007). The S_{hmin} value is taken from step-rate tests and fracture propagation analysis of PX-2. Further details of the preferred stress model are provided in in Chapter 4 of Korean Government Commission (2019) report.

We also consider an alternative model of stress based on the analysis of regional focal mechanisms recorded prior to the Pohang earthquake ("regional model"). The regional model corresponds to a strike-slip stress state and is based on the estimates of R and the azimuth of S_{Hmax} obtained by Soh *et al.* (2018), converted to principal stress magnitudes at a depth of 4.2 km assuming that $S_2 = S_v$, and that the state of stress is governed by frictional failure for a friction coefficient of 0.6.

Seismicity

A comprehensive reanalysis of the seismicity was undertaken as part of the Geological Society of Korea's investigation of the earthquake. A 1-D seismic velocity model based on check-shot data, PX-2 sonic logs and the borehole stratigraphy was constructed and augmented with regional seismological observations to form the composite model used to determine the location of the seismic activity (Korean Government Commission, 2019). A precise calibration of earthquake locations derived from the model was performed using data from a multi-level seismic array installed in PX-2 during the August 2017 stimulation of PX-1.

Seismic waveform data were collected from all available seismic stations within 80 km of the site, and earthquakes in addition to those in the EGS project and KMA catalog were identified using a matched filter. Earthquake hypocenters were determined from a combination of phase arrival time readings and waveform cross-correlation measurements. New magnitudes were determined using a calibrated local magnitude scale (M_L). In addition, moment magnitudes (M_W) were computed for many of the events. Further information on the two magnitude scales and their interrelation can be found in Figure 5-6 and Table A-3 of the Korean Government Commission (2019) report on the earthquake.

A total of 519 earthquakes were detected between January 1, 2009 and the time of the Pohang mainshock (Figure 4). More than half of these events (277) locate further than 10 km from the EGS project drill site. Of the 239 events spatially associated with the drill site, the earliest occurred on November 1, 2015. High-precision earthquake hypocenters were determined for 98 of these events.

The temporal characteristics of seismicity that occurred before drilling, while PX-1 and PX-2 were being drilled, and after completion when they were stimulated by high-pressure injection of water are the key factors for understanding the origin of the November 15, 2017, M_W 5.5 Pohang mainshock.

Seismicity Near the EGS Site Prior to Simulation

The analysis of the instrumental seismicity recorded by KMA shows that no instrumental seismicity with M_L > 2.0 has been detected within 10 km distance of the Pohang EGS site from at least 1978 to October 2015 (Kim *et al.*, 2018c). Only six events of M_L 1.2–1.9 had been detected in the area since 2006. In addition, Kim *et al.* (2018c) used a matched-filter technique to identify uncatalogued earthquakes in the continuous waveform data at station PHA2 of the KMA permanent network. PHA2 is located about 10 km north of the EGS site. The matched-filter analysis revealed no events near the Pohang EGS site for the period from January 2012 to October 2015. However, the analysis detected small earthquakes in the month of November 2015 that originated near the EGS project at the time when the PX-2 well was being drilled.

As part of the official investigation into the earthquake a new matched-filter search was conducted for events located near the Pohang EGS site using 40 templates representing all stimulations, foreshocks and the mud loss event. Six previously unidentified earthquakes were found within a 10 km radius of the site between January 2009 and October 2015 (Figure 4). The largest, M_L 2.2, occurred in March 2013 at a depth of 12 km. None were closer than 7 km to the bottom of PX-2 and they had depths of between 6 and 15 km. This analysis confirms that no earthquakes occurred in the vicinity of the crustal volumes stimulated by injection into PX-1 and PX-2 between January 2009 and November 2015. It also establishes that the mid-crust beneath the site was at least weakly seismogenic with tectonic earthquakes.

On September 12, 2016, the M_L 5.8 (M_W 5.4) Gyeongju earthquake occurred approximately

40 km south of Pohang within the major right-lateral Yangsan fault system. Grigoli *et al.* (2018) addressed the possibility that the Gyeongju earthquake might have contributed to triggering the Pohang earthquake, and concluded that the static Coulomb stress perturbation produced by the Gyeongju event on the Pohang fault was negligible, and that a direct triggering effect could be excluded.

From these analyses we conclude that no increase of seismicity in the area of the Pohang EGS project is observed prior to November 2015.

Seismicity Induced by Mud Loss during Drilling

Beginning on October 29, 2015, during the drilling of PX-2, the fault zone described above was encountered near 3,800 m depth (Figure 3). A significant loss of heavy drilling mud (density 1.6 g/cm^3) occurred at this time and in the following days, amounting to over 600 m^3 transferring an additional pressure of >20 MPa to the formation due to the weight of the mud column. The seismicity detected at station PHA2 started at this time and lasted through the month, with the largest event, M_L 0.8, occurring on November 30, 2015 (Figure 2; see also Figures A-2-1 and A-2-2 in Korean Government Commission (2019)). Of these events, we have only been able to locate the November 30 event.

The seismicity associated with mud loss from PX-2 indicates that the stress perturbation was sufficient to induce fault slip and implies that some faults were close to failure prior to stimulation. Further, it suggests that a hydraulically conductive structure was intersected near 3,800 m in PX-2. Previous mud loss of 76 m^3 in PX-1 at a depth of 3,400–3,500 m during the first phase of drilling and mud loss of <40 m^3 in PX-2 at a depth of 3,000–3,100 m in early October 2015 were not associated with discernible seismicity ($M_L \geq -0.5$). Mud loss of ~200 m^3 in PX-1 at a depth of 4,200–4,300 m in November 2016 also did not induce seismicity.

Seismicity Induced during EGS Stimulations

Earthquakes large enough to be located precisely occurred during each of the five well stimulations. The earthquakes define two distinct spatial populations that are related to well stimulation activities. Earthquakes that occurred during or shortly after stimulation of PX-1 fall into one population, while those that occurred during or shortly after stimulation of PX-2 fall into the other (Figure 5). Seismicity continues after individual stimulations of PX-2 ended, sometimes for weeks (Figure 2). The mud loss event discussed above locates together with the PX-2 events.

The range of focal depths of earthquakes associated with the well stimulations is very restricted (Figure 5). For earthquakes associated with PX-1, depths range between 3.7 and 4.4 km, a similar depth interval to the open-hole section of PX-1 (3.9~4.2 km). Earthquakes associated with PX-2 span the depth range from 3.8 to 4.4 km, compared with the open-hole interval from 4.2 to 4.3 km. Earthquakes in each zone exhibit both upward and downward growth with respect to the open-hole intervals where pressure entered the formation.

We discuss the seismicity associated specifically with PX-2 (which underwent the first, third and fifth stimulations) and PX-1 (the second and fourth stimulations) in the following sections.

Seismicity Associated with PX-2

The seismicity in the PX-2 cluster forms a tabular body striking 214°and dipping 43°to the NW. The zone has a strike length of 1000 m, dip length of 500 m and a width of 200 m. The best-fitting plane to the zone intersects PX-2 at 3,800 m depth. Most of the earthquakes locate within ±60 m of the plane. The earthquakes are projected onto the plane in Figure 6 (left) with the approximate area of each earthquake's rupture shown by a circular crack model with a radius appropriate for its magnitude. This plane is a good approximation of the structure of the seismicity.

The initial seismicity associated with the PX-2 cluster occurred during the drilling of the PX-2 well in November 2015, discussed above and as a consequence of the major mud loss event at 3,800 m depth. Of the eighteen detected earthquakes that occurred at the time of the mud loss, only the largest, M_L 0.8 on November 30, 2015 could be located with confidence (Figure 6). It locates near the top of the PX-2 cluster. No further activity was detected after well control was re-established and casing set until the first PX-2 stimulation in February 2016.

The first PX-2 stimulation produced only a modest seismic response (Figure 2), with the largest event being of M_W 1.6. More than 6 months after injection ended, a M_W 1.1 event occurred in the same cluster. The second PX-2 stimulation in March and April 2017 induced a M_W 3.2 earthquake on April 15, at a time when the well was shut in. The well was quickly opened and allowed to bleed off. It was followed by a robust aftershock sequence, with declining seismicity continued into mid-May (Figure 2). The third PX-2 stimulation in September 2017 produced only a modest seismic response, similar to the first stimulation, with a maximum magnitude event of M_W 2.0. The last earthquake large enough to be located occurred on September 26, 2017.

Forty-nine days later, on November 15, 2017, activity resumed in the PX-2 cluster with what proved to be the foreshocks of the Pohang earthquake. The foreshocks occurred immediately to the southwest of the area ruptured during the April 2017 stimulation. The largest and last locatable foreshock, M_W 2.7, occurred just 7 minutes before the mainshock and expanded the ruptured area down-dip toward the mainshock hypocenter (Figure 6). It is evident from the distribution of earthquakes in the PX-2 cluster that the Pohang mainshock initiated in an area that was strongly perturbed by not only the foreshocks but also by the entire sequence of earthquakes induced by injection into PX-2.

Focal mechanisms were obtained during this investigation for 53 earthquakes that occurred during and following the simulations and up until the M_W 5.5 earthquake on 15 November 2017 (Figure 7). The highest-quality focal mechanisms from the three phases of PX-2 stimulation exhibit predominantly oblique strike-slip/reverse faulting. Most of the events, including the largest earthquake during the stimulation (M_W 3.2 on April 15, 2017), have similar focal mechanisms to the foreshocks and the mainshock itself. This focal mechanism indicates oblique right-lateral slip on a NW-dipping plane or oblique left-lateral slip on the orthogonal E-dipping plane. The NW-dipping plane has a very similar geometry to the plane defined by PX-2 seismicity and to the fault plane of the M_W 5.5 inferred by analysis of regional moment tensor and InSAR analysis (Grigoli *et al.*, 2018). This plane is well-oriented for slip according to the preferred stress model.

Seismicity Associated with PX-1

Most of the earthquakes associated with PX-1 occurred during or shortly after the initial stimulation of the well in December 2016 (Figure 2). This stimulation activated an inclined tabular volume with a height of 800 m, horizontal length of 500 m and width of 230 m (Figure 6). Minor seismic activity continued in the zone following injection, with the last located event occurring in mid-January 2017. The second stimulation of the well in August 2017 produced only a single earthquake, M_W 1.2 that was large enough to locate with the surface seismic networks. This earthquake was also recorded by a multi-level borehole array deployed in PX-2 (Hofmann *et al.*, 2019). This earthquake could be precisely located using P-wave polarization angles and P-, S- and tube-arrival times on the array and was used to fix all absolute locations. A M_W 2.0 earthquake later occurred in the PX-1 zone four weeks after the stimulation ended. Thus, while the majority of activity occurred when the well was pressurized, seismicity lingered for weeks afterwards, as has been observed in many other hydraulic well stimulations (Yoon *et al.*, 2017).

Seismicity associated with stimulation of PX-1 shows a broad range of focal mechanisms (Figure 7). Many of the 21 highest-quality events have focal mechanisms similar to that characteristic of PX-2 seismicity, but other events show either purer strike-slip faulting (e.g. 08:04 event on 19 December 2016 and 07:56 event on 20 December 2016) or oblique strike-slip/reverse faulting on N- or S-dipping planes (e.g. 10:04 event on 21 December 2016). The orientation of the tabular zone of PX-1 seismicity is not represented in individual focal mechanisms (Figure 7).

M_W 5.5 Pohang Earthquake of 15 November 2017

In mid-November 2017, seismicity restarted on the fault activated by injection into PX-2 (Figure 6). The five largest events were recorded over a period of about 10 hours, between 19:55 on November 14 and 05:22 on November 15, with a magnitude progression increasing from M_W 1.6 to M_W 2.7. These events were immediately followed by the main M_W 5.5 shock, occurring at 05:29 on November 15.

Once initiated, the November 15, 2017 Pohang earthquake grew outward from its hypocenter and beyond the ~1000 m-long segment of the fault that had been activated by the stimulations of PX-2. The aftershock activity that followed the mainshock illuminated this plane further (Grigoli *et al.*, 2018; Kim *et al.*, 2018c) (Figure 8).

Discussion

Location and Timing of Mainshock

The mainshock of November 15, 2017 occurred 58 days after the last injection activities in PX-2. This delay has been used to argue that the mainshock has no causal connection to the

EGS activities in Pohang.

A delay of weeks and months between tectonic events occurring on adjacent fault segments is commonly observed, with seismic sequences developing in some cases over years and propagating to adjacent faults. A recent example is the sequence occurring in 2016 in the Central Apennines region of Italy, with four main episodes of seismicity occurring over several months (Chiaraluce *et al.*, 2017). The causal link in natural seismicity, even with delays of several months, is not disputed. A similar delay has also been observed in well-documented occurrences of induced seismicity, for example in the case of wastewater injection in Oklahoma (Keranen *et al.*, 2014; Schoenball and Ellsworth, 2017). The first documented case of earthquakes induced by injection occurred in the 1960s near Denver, Colorado, where a deep well was used to dispose of waste by injection at the Rocky Mountain Arsenal (Healy *et al.*, 1968). Injection into the Precambrian basement took place between March 1962 and February 1966, and the rate of injection was strongly correlated with the earthquake rate. However, the largest earthquake, M_W 4.8, struck in April 1967 more than one year after injection had been terminated. At Basel, Switzerland, activity continued for more than a year after pressure was bled off, with multiple magnitude 3 earthquakes occurring (Deichmann and Giardini, 2009).

On the basis of these observations, of both natural and induced seismicity, the separation in time between stimulation activities in PX-2 ending and the occurrence of the mainshock cannot be considered a reason to exclude a triggering effect of the EGS activities.

On the contrary, there are strong elements indicating a causal link between the seismicity induced by the PX-2 stimulations and the foreshocks and mainshock of November 2017. Indeed, the foreshocks (November 14, 2017, at 20:04 and 20:59) have the same waveform signature as the events that occurred during the last PX-2 stimulation (September 15, 2017, at

19:33; September 16, 2017, at 08:55), indicating that the PX-2 seismicity and the foreshocks are part of the same sequence of events and occurred on the same focal plane as the mainshock. The same correlation is not found for events associated with PX-1 stimulations. The foreshocks are contiguous with the previously ruptured area along the fault stimulated by injection into PX-2, extending the area approximately 200 m to the SW (Figure 6). The mainshock hypocenter sits immediately below the foreshocks, where stresses had been increased by the foreshocks and earlier events. From the location of the mainshock hypocenter alone, it is evident that this earthquake is directly related to the preceding activity.

Susceptibility to Slip in the Prevailing Stress Field

Figure 9 illustrates the orientations of key planes represented in the focal mechanisms and seismicity, and the corresponding shear and effective normal stresses calculated using the preferred stress model described above. This analysis indicates that planes with similar geometries to that of the mainshock fault plane (dipping towards the WNS at ~50°) were close to failure for the preferred stress model, such that small increases in fluid pressure would cause slip. In particular, the west-dipping nodal planes inferred from local network observations for the mainshock and the April 2017 M_W 3.2 event and the plane defined by PX-2 seismicity (planes 1, 3 and 5) were each near-optimally oriented for frictional reshear given the preferred stress model described above. Conversely, the east-dipping nodal planes of the mainshock and M_W 3.2 focal mechanisms, and the plane fit to PX-1 seismicity (planes 2, 4 and 6) were poorly oriented for shear in the prevailing stress field. The mainshock fault planes inferred from InSAR and moment tensor analysis by Grigoli *et al.* (2018) were also well-oriented for slip (planes 7 and 8). Similar results are obtained if the regional stress model is used.

In summary, the west-dipping nodal planes of the mainshock and M_W 3.2 event's focal mechanisms were close to failure whereas the respective auxiliary planes were not. Moreover, the plane defined by PX-2 seismicity, which has a very similar geometry to the mainshock fault plane, was also close to frictional failure for either of the stress models considered.

The inset in Figure 7 illustrates the observed focal mechanism representing the initiation of the mainshock and the focal mechanism calculated by resolving different stress models on the best-fitting plane fit to the PX-2 seismicity, assuming that slip occurs in the direction of maximum resolved shear stress. In each case, the calculated focal mechanism is similar to that observed, indicating oblique reverse/ strike-slip motion on the assumed west-dipping fault plane. For the preferred stress model, slip on this plane is calculated to have a rake of 141°, while the regional stress model yields a rake of 158°. Given uncertainties in the focal mechanism parameters and the stress models, the differences between the observed and predicted focal mechanisms are within acceptable bounds.

We conclude from this analysis that the two stress models considered are consistent with the geometry of slip during the mainshock. In other words, the mainshock focal mechanism, and the focal mechanisms of the foreshocks and several events associated with stimulation of PX-2, have a geometry that can be accounted for using a known fault geometry and plausible models of stress.

Effects of Tohoku and Gyeongju Earthquakes

The 2011 M_W 9.0 Tohoku earthquake produced small but measurable displacements across the Korean Peninsula (Kim and Bae, 2012). Sites on the eastern side of the Peninsula were displaced eastward by larger amounts than sites on the western side of the Peninsula, meaning that the induced strains were extensional; that is, the Korean Peninsula was stretched in an east–west direction. Hong *et al.* (2015) considered the changes in stress resulting from these geodetically measured strains and compared them with Coulomb failure stress perturbations. They obtained estimates of the tensional stress changes at mid-crustal depths of 1–7 kPa, which are of similar magnitude to the < 3 kPa reductions in Coulomb failure stress they calculated for optimally oriented strike-slip and reverse faults. In other words, the overall effect of the Tohoku earthquake on the Korean Peninsula was to slightly reduce the stresses causing strike-slip or reverse faulting on optimally oriented faults. This effect is referred to as a "stress shadow" as it reduces the potential for an earthquake to occur (Harris, 1998).

It has been suggested that the effect of the Tohoku earthquake had been to hasten the time of the M_L 5.1 (foreshock) and M_L 5.8 Gyeongju earthquakes in 2016 and that static stress perturbations caused by those events triggered the M_W 5.5 Pohang earthquake in 2017 (Hong *et al.*, 2018). This interpretation is based on the assertion that seismicity rates increased throughout the Korean region after 2011 and that the Gyeongju earthquakes increased Coulomb failure stresses near Pohang by ~200 Pa. This value is substantially smaller than previously observed triggering thresholds of order 0.01 MPa (Reasenberg and Simpson, 1992). In contrast, the Coulomb failure stress analysis by Grigoli *et al.* (2018) concluded that the Gyeongju earthquake did not play a role in triggering the Pohang earthquake 14 months later.

Hong *et al.* (2018) observed that no seismicity of magnitude 2 or larger was observed within 10 km of the 2017 earthquake's epicenter prior to the 2016 Gyeongju earthquakes, whereas four earthquakes of this size occurred within 3 km of the 2017 earthquake's epicenter after the 2016 earthquakes. They interpreted this to indicate that the Gyeongju earthquakes triggered low-magnitude seismicity near Pohang and ultimately the M_W 5.5 Pohang earthquake.

The occurrence of seismicity near the Pohang EGS site following the Gyeongju earthquakes and not before does not imply a causative relationship between the Gyeongju and Pohang earthquakes. On the contrary, the locations, timing, and focal mechanisms of the M_L 2+ earthquakes observed near Pohang in 2017 show that they were induced by EGS activities, as discussed above (Figures 2, Figures 5–7).

Hydrogeologic Modeling of Fluid Pressure Perturbations

Comprehensive analysis of the extent, timing, and magnitude of fluid pressure effects has yet to be undertaken and remains the topic of ongoing research. However, simple models provide a first-order characterization of the effects on fluid pressures of repeated stimulation.

The hydrogeologic regime surrounding the Pohang EGS site can be treated as the superposition of the pre-drilling state and any perturbations associated with drilling and injection. The models developed to date presume that an undisturbed, hydrostatic fluid pressure regime existed prior to stimulation, and therefore do not address the perturbations associated with the long phase of drilling or the mud loss event in October 2015.

Two models, referred to as Case A and Case B below, have been developed to illustrate key features of pore pressure diffusing away from the PX-1 and PX-2 injection intervals. Each model represents a 5 km × 5 km × 5 km domain and incorporates two faults (Figure 10). The faults are embedded in bedrock with a homogeneous hydraulic diffusivity of 1×10^{-2} m^2/s. The existence and geometries of the two faults are based on hydrologic analysis of the stimulation data and the seismological results described in Chapter 5 of Korean Government Commission (2019) report. The first fault separates PX-1 and PX-2 and represents the mainshock plane, having an orientation (strike/dip) of 214°/43°and intersecting PX-2 at 3,810 m. It acts to compartmentalize the fluid pressure response. The second fault represents a high-permeability feature inferred to be present near PX-1. The hydrologic properties of the faults have been specified on the basis of representative models of fault zone structure (Caine *et al.*, 1996; Choi *et al.*, 2015) and laboratory measurements of the fault gauge and breccia samples from lithologies analogous to the basement rock at Pohang (Kim *et al.*, 2018a).

- Case A: The mainshock fault plane is modeled as having a 10 m-thick low-permeability fault core (D= 1×10^{-6} m^2/s) bounded on both sides by a 85 m-thick high-permeability damage zone (D = 0.1 m^2/s) (Kim *et al.*, 2018a). The second fault is a smaller, 130 m-thick, high- permeability feature (D = 1 m^2/s) near PX-1.

- Case B: The fault locations and geometries are the same as in Case A but the mainshock fault plane does not have a low-permeability core.

The temporal evolution of pore pressure at the hypocenters of the M_W 3.2 and M_W 5.5 earthquakes is illustrated in Figure 10. The model results suggest that pore pressure had been elevated by 0.15–0.30 MPa at the hypocenter of the M_W 3.2 event by April 15, 2017, largely as a consequence of the third stimulation phase in PX-2. By November 15, 2017, the modeling suggests pore pressure had risen by approximately 0.07 MPa at the hypocenter of the M_W 5.5 earthquake. Pore pressure changes of more than 0.01 MPa have been shown to reduce fault strength and trigger earthquakes (Reasenberg and Simpson, 1992).

The geomechanical results presented above indicate that the mainshock fault plane was critically stressed prior to the Pohang earthquake, and imply that small increases in fluid pressure would trigger slip. More detailed analysis remains to be undertaken but the fluid pressure modeling conducted to date indicates that fluid pressure increases of greater than 0.01 MPa were likely to have occurred at distances of several hundred meters from the injection intervals and to have persisted for weeks or months after injection ended.

Magnitude of Mainshock and Previous Scaling Arguments

It has been argued that the sizes of earthquakes induced by stimulation can be managed by controlling the pressure, rate, volume and location at which fluid enters the rock mass and by allowing pressures to dissipate when seismicity rates escalate or magnitudes exceed pre-defined thresholds (Hofmann *et al.*, 2019). The threshold magnitudes for traffic light systems have often been set to avoid earthquakes that pose a shaking nuisance and/or risk of damage.

Part of the rationale for selecting the magnitude thresholds comes from an empirical hypothesis that the largest magnitude of induced earthquakes is bounded by a function of the injected volume (Galis *et al.*, 2017; McGarr, 2014). If correct, this "volume hypothesis" would enable the hazard to be managed prescriptively by simply maintaining the net injection volume below a certain value. However, an alternative analysis of the same cases found that the observed maximum magnitude was well modeled by independent random sampling of the Gutenberg-Richter distribution $\log_{10}(N) = a - bM$, where N is the cumulative number of events greater than or equal to M (van der Elst *et al.*, 2016). In this interpretation, the largest event in an induced seismicity sequence is not related to the injection volume, but to pre-existing tectonic conditions and the number of earthquakes induced. The greater the number of earthquakes, the higher the odds of one of those earthquakes being large.

The Pohang earthquake contradicts the volume hypothesis, as the injected volume was less than $1/500^{th}$ of the amount expected to produce a M_W 5.5 earthquake. This discrepancy would be larger if the net volume (injection minus extraction) were considered instead of injection alone. Once initiated, the Pohang earthquake grew through the release of tectonic stress rather than being limited by the injected volume. The earthquake was almost two magnitude units larger than the M_W 3.7 predicted by one model (McGarr, 2014) and exceeded the maximum "arrested" earthquake size predicted by the other (Galis *et al.*, 2017) and therefore constituted a "runaway" earthquake in their terminology, or "triggered" in the terminology of *Shapiro et* *al.* [2013] Shapiro *et al.* (2013).

Conclusions

The Pohang earthquake was triggered by the EGS stimulation of the PX-2 well. Seismicity induced by injection activated a previously unknown fault, which in turn triggered the mainshock (Figure 11). Once initiated, the earthquake grew through the release of tectonic strain. We summarize below the key findings that lead to this conclusion and end with lessons of a general nature that can serve to increase the safety of future EGS projects.

The Korean Peninsula is located on the continental margin of the Eurasian plate, which underwent extension during the opening of the East Sea. The region is now under tectonic compression and previously extensional faults with appropriate orientations can be reactivated with reverse or strike-slip kinematics. The present-day regional stress field shows compression oriented ENE–WSW and several recognized active fault systems in the region are susceptible to slip in this stress field. The stresses acting on regional faults are high, approaching the static stability of the faults, as confirmed by pre-drilling assessment of stress conditions in Pohang. The occurrence of the M_W 5.4 Gyeongju event of September 12, 2016, on the Yangsan fault system is consistent with this analysis.

The historical seismic record shows periods of high activity, including earthquakes exceeding the size of the 2016 Gyeongju and 2017 Pohang earthquakes. Regional deformation following the 2011 M_W 9.0 Tohoku earthquake may have affected seismic activity in the Korean Peninsula. However, the calculated effects of the regional deformation and the seismicity do not explain the occurrence of the Pohang earthquake.

Neither geological investigations in the Pohang area nor geophysical surveys performed during the selection of the EGS site identified the fault that ruptured in the Pohang earthquake. Fault gouge observed in drill cuttings from the PX-2 well indicates the presence of a fault at a depth of approximately 3,800 m.

Multiple lines of evidence suggest that the PX-1 and PX-2 wells occupy different hydraulic regimes. Injection tests carried out during hydraulic stimulations indicated the presence of a flow barrier separating the two wells. Two distinct seismicity populations, separated in space and time, were observed during successive stimulations of the PX-1 and PX-2 wells. A low-permeability gouge zone or zones encountered near 3,800 m in PX-2 may form a hydraulic barrier between the two wells. Injection conditions in the two wells were different, requiring a maximum well-head pressure of 24 MPa in PX-1 and almost 90 MPa in PX-2.

Modeling performed with representative hydrological properties and high-permeability and low-permeability fault cores shows that the pressure perturbations produced by stimulation of PX-2 propagated several hundred meters. The pore pressure increases near the hypocenters of the M_W 3.2 and M_W 5.5 events exceeded 0.05 MPa. Detectable seismicity occurred during drilling of PX-2 over a period of one month, following the mud loss event at about 3,800 m depth, induced by the weight of the mud column entering the formation.

Each of the five stimulations induced seismicity. After each stimulation in PX-2 seismicity continued for up to several months. The seismicity induced by the stimulations ranges in depth between 3.7 and 4.4 km, spanning the open sections of the two boreholes (Figure 11). Seismicity induced by the three stimulations in PX-2 did not produce a detectable seismic response within 200 m of the well but activated an approximately 1000 m-long, 600 m-high fault zone aligned with the fault traversing PX-2 at 3,800 m and corresponding to the west-dipping plane of the M_W 5.5 Pohang mainshock focal mechanism.

The west-dipping nodal planes of the focal mechanisms of events induced by PX-2 injection agree with the orientation of the stimulated fault zone. Their oblique reverse motion is well explained by the local stress field. The orientation of the fault activated by the mainshock is similar to that of other faults in the region. The geometry of the initial slip in the mainshock is well explained by the combination of the fault geometry and the state of stress surrounding the borehole.

The mainshock was preceded by foreshocks over a period of 24 hours, with a sequence of events of increasing size culminating in an event of M_W 2.7 seven minutes before the mainshock. These foreshocks extended laterally the fault zone activated by seismicity induced by PX-2 stimulations. They have similar focal mechanisms to the mainshock and the events induced by the PX-2 stimulations.

The mainshock initiated within the fault zone activated by the PX-2 stimulations, at 4.3 km depth. The delay of almost two months between the last PX-2 stimulated events and the mainshock is consistent with similar delays observed in earlier stimulations in Pohang and commonly observed in natural and induced seismic sequences. A delay of this length does not preclude a causal effect.

The size of the mainshock is consistent with a triggered origin according to the published analyses of van der Elst *et al.* (2016) and Galis *et al.* (2017), and is inconsistent with the hypotheses of McGarr (2014) or Galis *et al.* (2017) that relate the maximum magnitude of an induced earthquake to the injected volume.

Lessons Learned

The Pohang earthquake was triggered by the EGS stimulation. Seismicity induced by injection activated a previously unmapped fault zone, which in turn triggered the mainshock. Lessons of a general nature can be learned from the Pohang experience, and serve to increase the safety of future EGS projects in Korea and elsewhere. Further analysis of the implications of the Pohang experience for managing injection-induced seismic risks in other situations has been described by Lee *et al.* (2019).

The Pohang event had a complex origin. Current models do not cover adequately this complexity and the possibility that pressure perturbations induced on a fault may trigger run-away events of large magnitudes. Physical and statistical models of induced and triggered seismicity need to be further developed to provide reliable assessments of probabilities and uncertainties for inclusion in risk assessments of future EGS projects.

The analyses and investigations referenced in this report were done only after the occurrence of the M_W 5.5 Pohang mainshock, but they would have been possible during the sequence of stimulations, lasting almost two years. All the data required to re-evaluate seismic risk were collected and the most important evidence was available in April 2017 after the second stimulation in PX-2. In future EGS projects, the project team and the scientific institutions involved should engage in timely and adequate efforts to monitor, analyze and understand the evolution of any earthquake sequence, and provide information to the public authorities on the developing seismic risk conditions.

Several institutions from Korea and other countries were active in different capacities in the monitoring and analysis of the seismicity in Pohang. This complicated the exchange and analysis of data and samples. Scientific institutions involved in monitoring and evaluation activities with relevance to the assessment and mitigation of seismic risk — such as the risk potentially associated with an EGS project in the vicinity of a major city — should prioritize an open-access policy for data and samples and clear channels of cooperation to maximize their contribution to the mitigation of seismic risk.

The Pohang EGS project was located close to a major city, port and industrial center, with more than 200 high-rise apartment buildings within 5 km of the EGS site. This proximity should have raised clear issues of seismic risk, governance and mitigation. It is crucial that strategies and tools for monitoring, mitigating and communicating the risk of induced seismicity are established together with responsible authorities. Seismic risk scenarios should be developed to evaluate the possible consequences and to identify risk mitigation measures. A risk-based framework for making operational decisions should always be used and updated as new knowledge is acquired.

Operational decision-making in the EGS project was internal to the project team. An independent oversight committee/authority should be established to provide assurance that all aspects of the project plan, protocols and standards are designed and conducted with appropriate considerations of seismic risk.

Data and Resources

All of the data used in our work were produced as part of the Korean Government investigation into the cause of the 2017 Pohang Earthquake (Korean Government Commission, *2019*). That report is available online at https://doi.org/10.22719/KETEP-20183010111860.

Acknowledgements

We gratefully acknowledge valuable discussions and interactions with Kang-Kun Lee, In-Wook Yeo, Jeong-Un Woo, Chandong Chang, Dong-Hoon Sheen, Junkee Rhie, Tae-Seob Kang, Min-Wook Kim, Francesco Grigoli, Kwang-Hee Kim, Peter Meier, Falko Bethmann and Cornelius Langenbruch. Martin Galis and an anonymous reviewer provided helpful comments during the review process. The cooperation of NexGeo, KIGAM and Geo-Energie

Suisse in providing data and results during this study are also gratefully appreciated.

References

Caine, J. S., J. P. Evans, and C. B. Forster (1996). Fault zone architecture and permeability structure, *Geology*, **24**, no. 11, 1025-1028, doi: 10.1130/0091-7613(1996)024<1025:FZAAPS>2.3.CO;2.

Cheon, Y., M. Son, C. W. Song, J. S. Kim, and Y. K. Sohn (2012). Geometry and kinematics of the Ocheon Fault System along the boundary between the Miocene Pohang and Janggi basins, SE Korea, and its tectonic implications, *Geosci. J.*, **16**, no. 3, 253-273, doi: 10.1007/s12303-012-0029-0.

Chiaraluce, L., et al. (2017). The 2016 central Italy seismic sequence: A first look at the mainshocks, aftershocks, and source models, *Seis. Res. Lett.*, **88**, no. 3, 757-771, doi: 10.1785/0220160221.

Choi, J. H., S. J. Yang, S. R. Han, and Y. S. Kim (2015). Fault zone evolution during Cenozoic tectonic inversion in SE Korea, *J. Asian Earth Sci.*, **98**, no., 167-177, doi: 10.1016/j.jseaes.2014.11.009.

Chough, S. K., S. T. Kwon, J. H. Ree, and D. K. Choi (2000). Tectonic and sedimentary evolution of the Korean peninsula: A review and new view, *Earth Sci. Rev.*, **52**, no. 1-3, 175-235, doi: 10.1016/S0012-8252(00)00029-5.

Deichmann, N., and D. Giardini (2009). Earthquakes Induced by the stimulation of an enhanced geothermal system below Basel (Switzerland), *Seis. Res. Lett.*, **80**, no. 5, 784-798, doi: 10.1785/gssrl.80.5.784.

Ellsworth, W. L. (2013). Injection-induced earthquakes, *Science*, **341**, no. 6142, doi: 10.1126/science.1225942.

Galis, M., J. P. Ampuero, P. M. Mai, and F. Cappa (2017). Induced seismicity provides insight into why earthquake ruptures stop, *Science Adv.*, **3**, no. 12, doi: 10.1126/sciadv.aap7528.

Grigoli, F., S. Cesca, E. Priolo, A. P. Rinaldi, J. F. Clinton, T. A. Stabile, B. Dost, M. G. Fernandez, S. Wiemer, and T. Dahm (2017). Current challenges in monitoring, discrimination, and management of induced seismicity related to underground industrial activities: A European perspective, *Rev. Geophys.*, **55**, no. 2, 310-340, doi: 10.1002/2016RG000542.

Grigoli, F., S. Cesca, A. P. Rinaldi, A. Manconi, J. A. López-Comino, J. F. Clinton, R. Westaway, C. Cauzzi, T. Dahm, and S. Wiemer (2018). The November 2017 M_w5.5 Pohang earthquake: A possible case of induced seismicity in South Korea, *Science*, **360**, no. 6392, 1003-1006, doi: 10.1126/science.aat2010.

Harris, R. A. (1998). Introduction to special section: Stress triggers, stress shadows, and implications for seismic hazard, *J. Geophys. Res. Solid Earth*, **103**, no. 10, 24347-24358, doi.

Healy, J. H., W. W. Rubey, D. T. Griggs, and C. B. Raleigh (1968). The Denver earthquakes, *Science*, **161**, no. 3848, 1301-1310, doi: 10.1126/science.161.3848.1301.

Hofmann, H., et al. (2019). First field application of cyclic soft stimulation at the Pohang Enhanced Geothermal System site in Korea, *Geophys. J. Int.*, **217**, no. 2, 926-949, doi: 10.1093/gji/ggz058.

Hong, T. K., J. Lee, and S. E. Houng (2015). Long-term evolution of intraplate seismicity in stress shadows after a megathrust, *Phys. Earth Planet. In.*, **245**, no., 59-70, doi: 10.1016/j.pepi.2015.05.009.

Hong, T. K., J. Lee, W. Kim, I. K. Hahm, N. C. Woo, and S. Park (2017). The 12 September 2016 M_L5.8 midcrustal earthquake in the Korean Peninsula and its seismic implications, *Geophys. Res. Lett.*, **44**, no. 7, 3131-3138, doi: 10.1002/2017GL072899.

Hong, T. K., J. Lee, S. Park, and W. Kim (2018). Time-advanced occurrence of moderate-size earthquakes in a stable intraplate region after a megathrust earthquake and their seismic properties, *Sci. Rep.*, **8**, no. 1, doi: 10.1038/s41598-018-31600-5.

Houng, S. E., and T. K. Hong (2013). Probabilistic analysis of the Korean historical earthquake records, *Bull. Seis. Soc. Am.*, **103**, no. 5, 2782-2796, doi: 10.1785/0120120318.

Keranen, K. M., M. Weingarten, G. A. Abers, B. A. Bekins, and S. Ge (2014). Sharp increase in central Oklahoma seismicity since 2008 induced by massive wastewater injection, *Science*, **345**, no. 6195, 448-451, doi: 10.1126/science.1255802.

Kim, H., L. Xie, K.-B. Min, S. Bae, and O. Stephansson (2017). Integrated in situ stress estimation by hydraulic fracturing, borehole observations and numerical analysis at the EXP-1 borehole in Pohang, Korea, *Rock Mech. Rock Eng.*, **50**, no. 12, 3141-3155, doi: 10.1007/s00603-017-1284-1.

Kim, J. H., J.-H. Ree, C. Park, C.-M. Kim, R. Han, and T. K. Shimamoto, H.-C. (2018a). Proxies for the 2017 Pohang earthquake fault and modeling of fluid flow (S23B-0519), in *AGU Fall Meeting Abstracts*, edited, Washington, D.C., doi.

Kim, K. H., et al. (2018b). Deep fault plane revealed by high-precision locations of early aftershocks following the 12 September 2016 M_l5.8 Gyeongju, Korea, earthquake, *Bull. Seis. Soc. Am.*, **108**, no. 1, 517-523, doi: 10.1785/0120170104.

Kim, K. H., J. H. Ree, Y. Kim, S. Kim, S. Y. Kang, and W. Seo (2018c). Assessing whether the 2017 Mw5.4 Pohang earthquake in South Korea was an induced event, *Science*, **360**, no. 6392, 1007-1009, doi: 10.1126/science.aat6081.

Kim, S. K., and T. S. Bae (2012). Analysis of crustal deformation on the Korea peninsula after the 2011 Tohoku earthquake, *J. Kor. Soc. Surv. Geod. Photo. Cart.*, **30**, no. 1, 87-96, doi: 10.7848/ksgpc.2012.30.1.087.

Kim, Y. H., J. Rhie, T. S. Kang, K. H. Kim, M. Kim, and S. J. Lee (2016). The 12 September 2016 Gyeongju earthquakes: 1. Observation and remaining questions, *Geosci. J.*, **20**, no. 6, 747-752, doi: 10.1007/s12303-016-0033-x.

Korean Government Commission (2019). Summary report of the Korean Government Commission on relations between the 2017 Pohang Earthquake and EGS Project, edited, Geological Survey of Korea, Seoul, doi: 10.22719/KETEP-20183010111860.

Lee, H., Y. J. Shinn, S. H. Ong, S. W. Woo, K. G. Park, T. J. Lee, and S. W. Moon (2017a). Fault reactivation potential of an offshore CO_2 storage site, Pohang Basin, South Korea, *J. Petrol. Sci. Eng.*, **152**, no., 427-442, doi: 10.1016/j.petrol.2017.03.014.

Lee, J., T. K. Hong, and C. Chang (2017b). Crustal stress field perturbations in the continental margin around the Korean Peninsula and Japanese islands, *Tectonophysics*, **718**, no., 140-149, doi: 10.1016/j.tecto.2017.08.003.

Lee, J., et al. (2018). Seismicity of the 2016 M_L 5.8 Gyeongju earthquake and aftershocks in South Korea, *Geosci. J.*, **22**, no. 3, 433-444, doi: 10.1007/s12303-017-0071-z.

Lee, K.-K., et al. (2019). Managing injection-induced seismic risks, *Science*, **364**, no. 6442, 730-732, doi: 10.1126/science.aax1878.

Lee, K., and W. S. Yang (2006). Historical seismicity of Korea, *Bull. Seis. Soc. Am.*, **96**, no. 3, 846-855, doi: 10.1785/0120050050.

Lee, T. J., Y. Song, D.-W. Park, J. Jeon, and W. S. Yoon (2015). Three dimensional geological model of Pohang EGS pilot site, Korea, paper presented at Proceedings of the World Geothermal Congress, Melbourne, Australia, 19-25 April 2015.

Lee, Y., S. Park, J. Kim, H. C. Kim, and M. H. Koo (2010). Geothermal resource assessment in Korea, *Renew. Sustain. Energ. Rev.*, **14**, no. 8, 2392-2400, doi: 10.1016/j.rser.2010.05.003.

McGarr, A. (2014). Maximum magnitude earthquakes induced by fluid injection, *J. Geophys. Res. Solid Earth*, **119**, no. 2, 1008-1019, doi: 10.1002/2013JB010597.

Park, J. C., W. Kim, T. W. Chung, C. E. Baag, and J. H. Ree (2007). Focal mechanisms of recent earthquakes in the Southern Korean Peninsula, *Geophys. J. Int.*, **169**, no. 3, 1103-1114, doi: 10.1111/j.1365-246X.2007.03321.x.

Reasenberg, P. A., and R. W. Simpson (1992). Response of regional seismicity to the static stress change produced by the Loma Prieta earthquake, *Science*, **255**, no. 5052, 1687-1690, doi: 10.1126/science.255.5052.1687.

Ree, J. H., and S. T. Kwon (2005). The Wangsan Fault: One of the most 'active' faults in South Korea?, *Geosci. J.*, **9**, no. 3, 223-226, doi: 10.1007/BF02910581.

Ree, J. H., Y. J. Lee, E. J. Rhodes, Y. Park, S. T. Kwon, U. Chwae, J. S. Jeon, and B. Lee (2003). Quaternary reactivation of tertiary faults in the southeastern Korean Peninsula: Age constraint by optically stimulated luminescence dating, *Island Arc*, **12**, no. 1, 1-12, doi: 10.1046/j.1440-1738.2003.00372.x.

Schoenball, M., and W. L. Ellsworth (2017). A systematic assessment of the spatiotemporal evolution of fault activation through induced seismicity in Oklahoma and Southern Kansas, *J. Geophys. Res. Solid Earth*, **122**, no. 12, 10189-10206, doi: 10.1002/2017JB014850.

Shapiro, S. A., O. S. Krüger, and C. Dinske (2013). Probability of inducing given-magnitude earthquakes by perturbing finite volumes of rocks, *J. Geophys. Res. Solid Earth*, **118**, no. 7, 3557-3575, doi: 10.1002/jgrb.50264.

Soh, I., C. Chang, J. Lee, T. K. Hong, and E. S. Park (2018). Tectonic stress orientations and magnitudes, and friction of faults, deduced from earthquake focal mechanism inversions over the Korean Peninsula, *Geophys. J. Int.*, **213**, no. 2, 1360-1373, doi: 10.1093/gji/ggy061.

Son, M., C. W. Song, M.-C. Kim, Y. Cheon, H. Cho, and Y. K. Sohn (2015). Miocene tectonic evolution of the basins and fault systems, SE Korea: dextral, simple shear during the East Sea (Sea of Japan) opening, *J. Geol. Soc.*, **172**, no. 5, 664-680, doi: 10.1144/jgs2014-079.

Townend, J., and M. D. Zoback (2000). How faulting keeps the crust strong, *Geology*, **28**, no. 5, 399-402, doi: 10.1130/0091-7613(2000)28<399:hfktcs>2.0.co;2.

van der Elst, N. J., M. T. Page, D. A. Weiser, T. H. W. Goebel, and S. M. Hosseini (2016). Induced earthquake magnitudes are as large as (statistically) expected, *J. Geophys. Res. Solid Earth*, **121**, no. 6, 4575-4590, doi: 10.1002/2016JB012818.

Yoon, C. E., Y. Huang, W. L. Ellsworth, and G. C. Beroza (2017). Seismicity during the initial stages of the Guy-Greenbrier, Arkansas, earthquake sequence, *J. Geophys. Res. Solid Earth*, **122**, no. 11, 9253-9274, doi: 10.1002/2017JB014946.

Zoback, M. D. (2007). *Reservoir geomechanics*, 449 pp., Cambridge University Press, Cambridge.

William L. Ellsworth
Department of Geophysics
Stanford University
397 Panama Mall
Stanford, California 94035, U.S.A
wellsworth@stanford.edu

Domenico Giardini
Energy Science Center
Department of Earth Sciences
ETH Zürich
Sonneggstrasse 5
8092 Zürich, Switzerland

John Townend
School of Geography, Environment and Earth Sciences
Victoria University of Wellington
PO Box 600
Wellington 6140, New Zealand

Shemin Ge
Department of Geological Sciences
University of Colorado Boulder
UCB 399
Boulder, Colorado 80309, U.S.A.

Toshihiko Shimamoto
State Key Laboratory of Earthquake Dynamics
Institute of Geology
China Earthquake Administration
Beijing 100029, China

Figures

Figure 1. (Left) Aerial photograph showing the location of the Pohang Enhanced Geothermal System (EGS) drill-site; the inset shows the regional setting. (Right) Schematic diagrams of the two exploration wells PX-1 and PX-2.

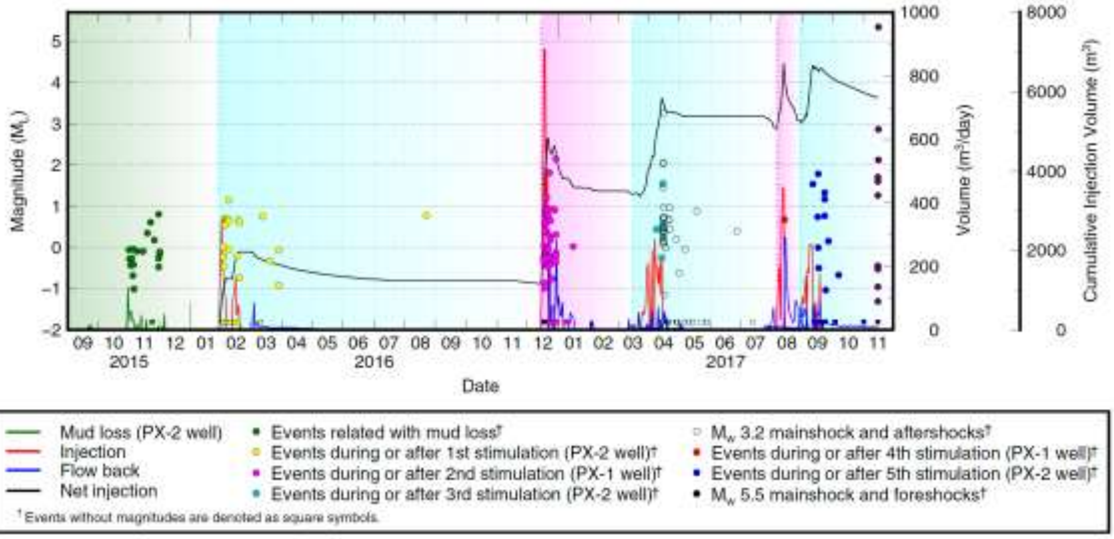

Figure 2. Timeline of the Pohang EGS stimulations and seismicity leading up to the November 15, 2017 M_W 5.5 Pohang earthquake. The six shaded periods represent, in sequence, the November 2015 mud loss, the first stimulation (in PX-2), the second stimulation (in PX-1), the third stimulation (in PX-2), the fourth stimulation (in PX-1), and the fifth stimulation (in PX-2). Earthquakes with measured local magnitudes (M_L) are represented by colored dots (left-hand scale). Daily injection and flow-back volumes and the cumulative net injection volume are illustrated with colored lines (right-hand scales). The largest event, M_L 3.2, occurred during the second stimulation of PX-2 in April 2017 when the pumps were off. This event and its aftershocks are plotted as open circles to distinguish them from events in green that occurred during injection into the well. Note the position of the M_L 3.2 event just below the cumulative volume curve.

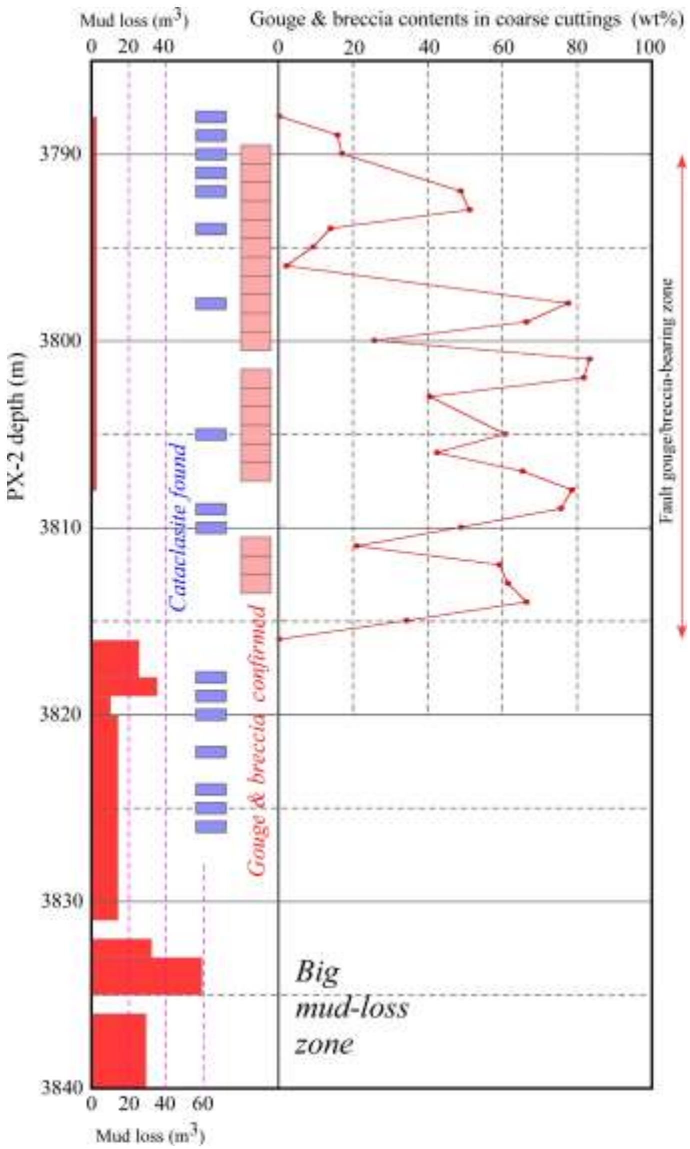

Figure 3. Summary of fault rocks and mud-loss data for the depths of 3,785–3,840 m in the PX-2 borehole, revealing a large-scale fault. The contents of fault gouge and breccia were determined for cuttings greater than a few millimeters in size at each depth. The mud-loss data were quoted from an unpublished compilation of drilling data by Geo-Energie Suisse.

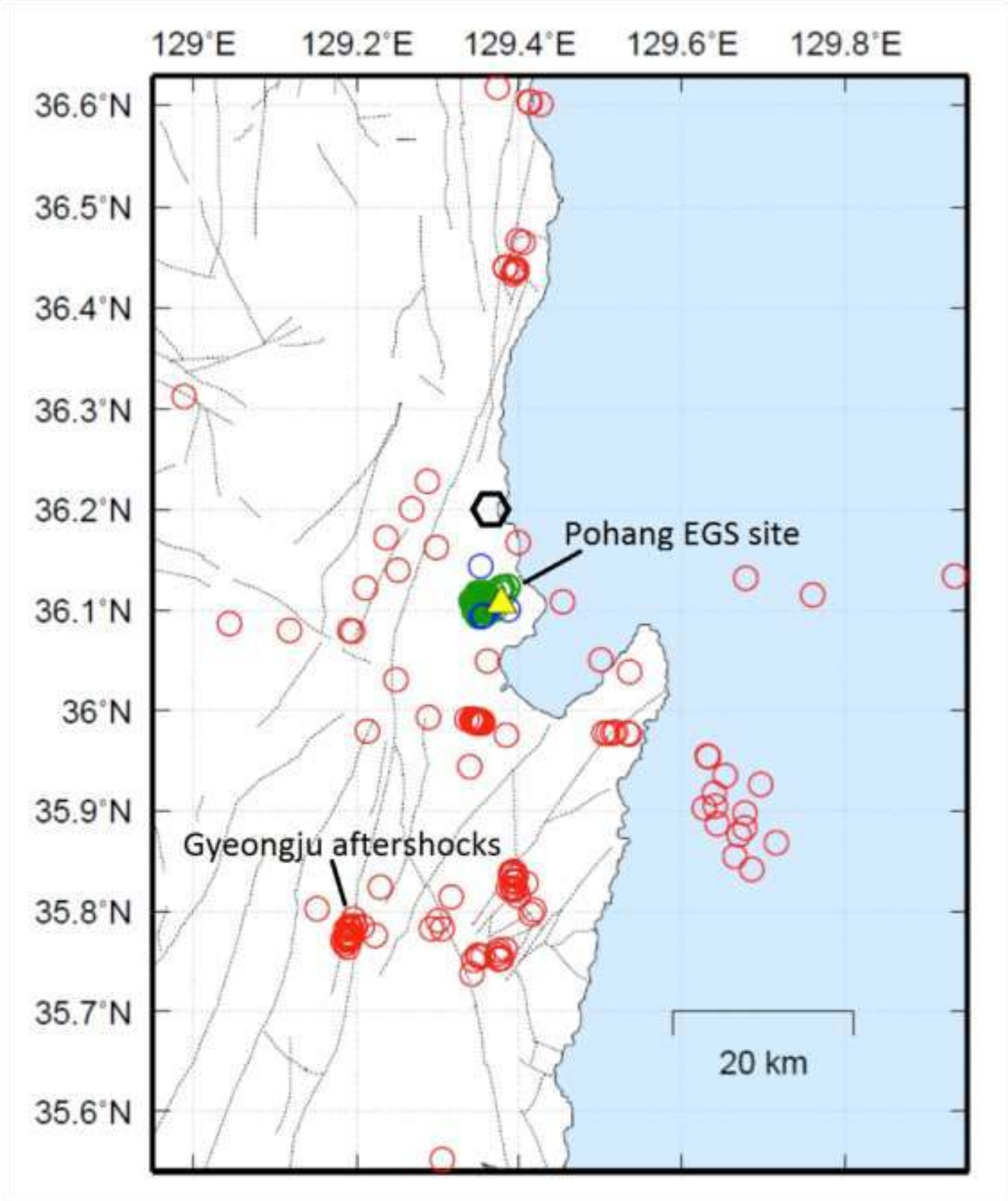

Figure 4. Epicentral distribution of 519 earthquakes detected between January 1, 2009 and November 15, 2017 in the Pohang region. Earthquakes within 10 km of EGS project drill site (yellow triangle) and shallower than 10 km are shown in green, and the four deeper than 10 km in blue; earthquakes further than 10 km from the drill site are shown in red. Location of permanent seismic station PHA2 shown by black hexagon.

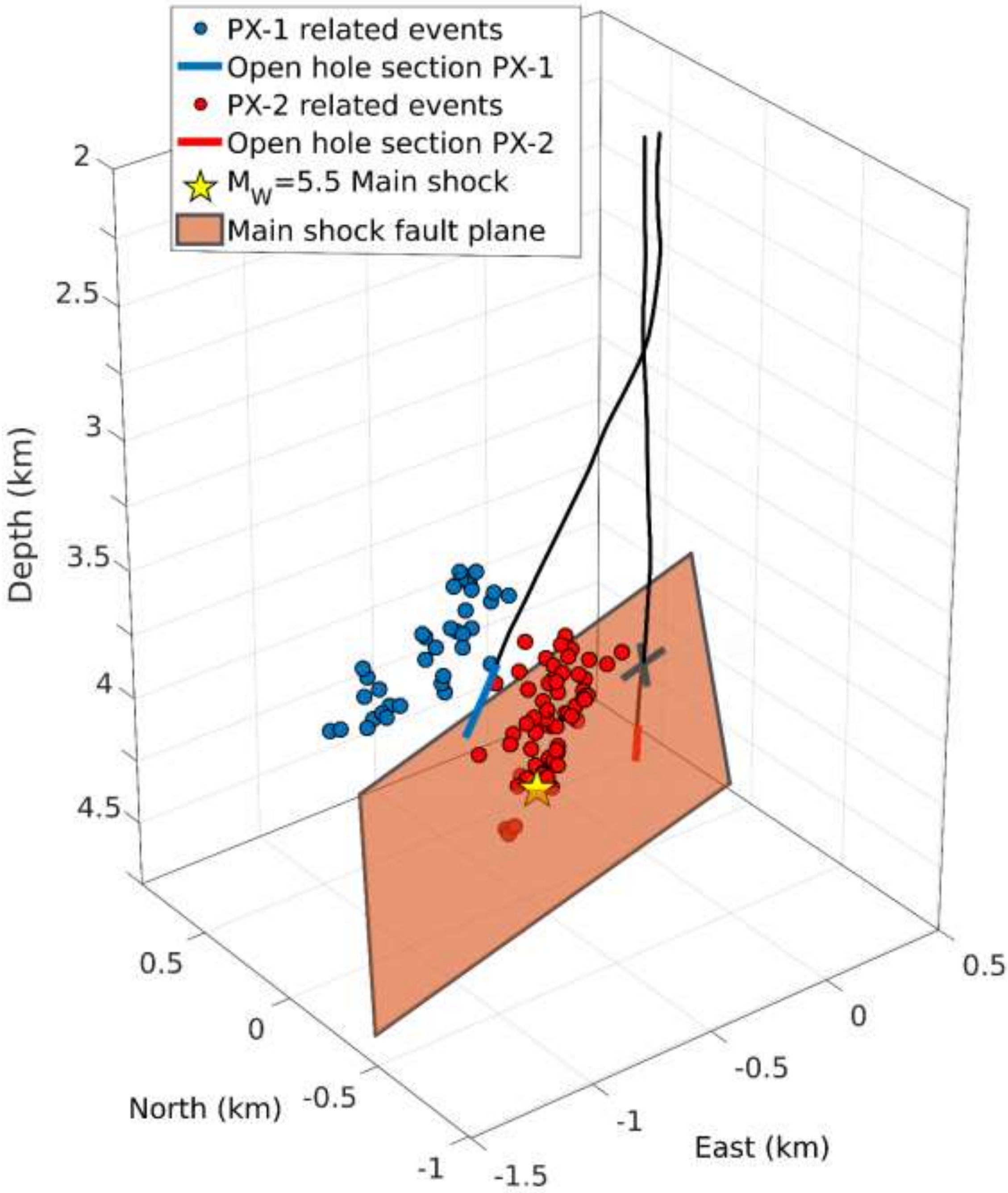

Figure 5. Perspective view of earthquakes associated with activity in PX-1 (blue) and PX-2 (red). Yellow star marks the mainshock hypocenter. Well trajectories are shown with the open hole sections for PX-1 and PX-2 in blue and red, respectively. Mainshock fault plane intersects PX-2 at 3.8 km depth and is marked by “X”.

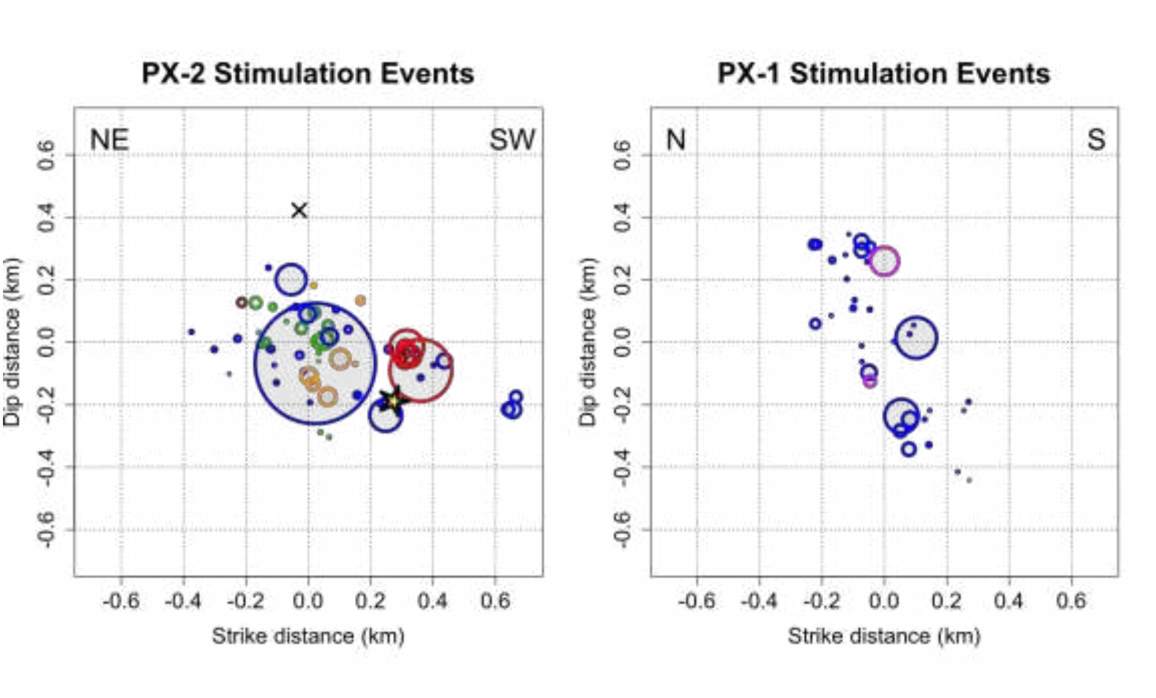

Figure 6. Earthquakes associated with (left) PX-2 injection and (right) PX-1 injection, projected onto the best-fitting plane in each case. For PX-2, the bottom of the open-hole section of the well is at (0,0), 375 m behind the plane and the intersection of the plane with the well at 3.8 km depth is marked by ×; the mud loss event in November 2015 is shown in brown, events during and following first stimulation in February 2016 in green, events during and following second stimulation in April 2017 in blue, events during and following third stimulation in September 2017 in orange, and foreshocks on November 14 and 15 in red. For PX-1, the coordinates are relative to the center of the seismicity; earthquakes during and following the December 2016 stimulation are shown in blue, earthquakes during and following the August 2017 stimulation in magenta. For both images, the faulted area in each earthquake is approximated by the equivalent circular crack for a stress drop of 4 MPa. This value for stress drop is the global average for crustal earthquakes [*Allmann and Shearer*, 2009]. *Song and Lee* [2018] estimated the stress drop of the Pohang mainshock in the region near the hypocenter to be in the range from 2 to 4 MPa.

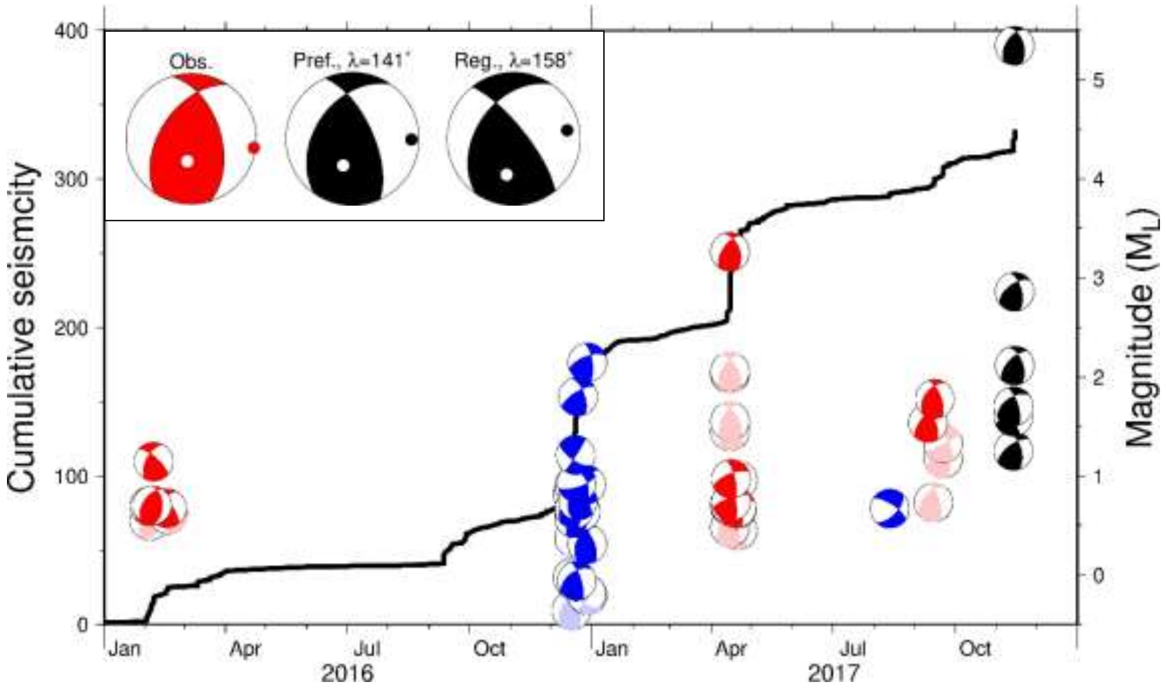

Figure 7. Summary of the P-wave focal mechanisms computed for 53 events that occurred during the five phases of stimulation (red — PX2; blue — PX-1), the foreshocks of 14–15 November 2017, and the M_W 5.5 Pohang earthquake (black). Bright red and blue colors indicate the highest-quality focal mechanism solutions associated with PX-2 and PX-1, and the paler colors indicate poorer-quality solutions. The inset in the top-left corner shows the observed mainshock focal mechanism (red beachball; strike/dip/rake = 214°/51°/128°) and focal mechanisms calculated using the PX-2 seismicity plane and preferred ("Pref.") and regional ("Reg.") models of stress (black beachballs). The value of the rake (λ) calculated for each of the stress models is printed above the corresponding beachball. For each focal mechanism, the white dot marks the T axis and the red or black dot the P axis.

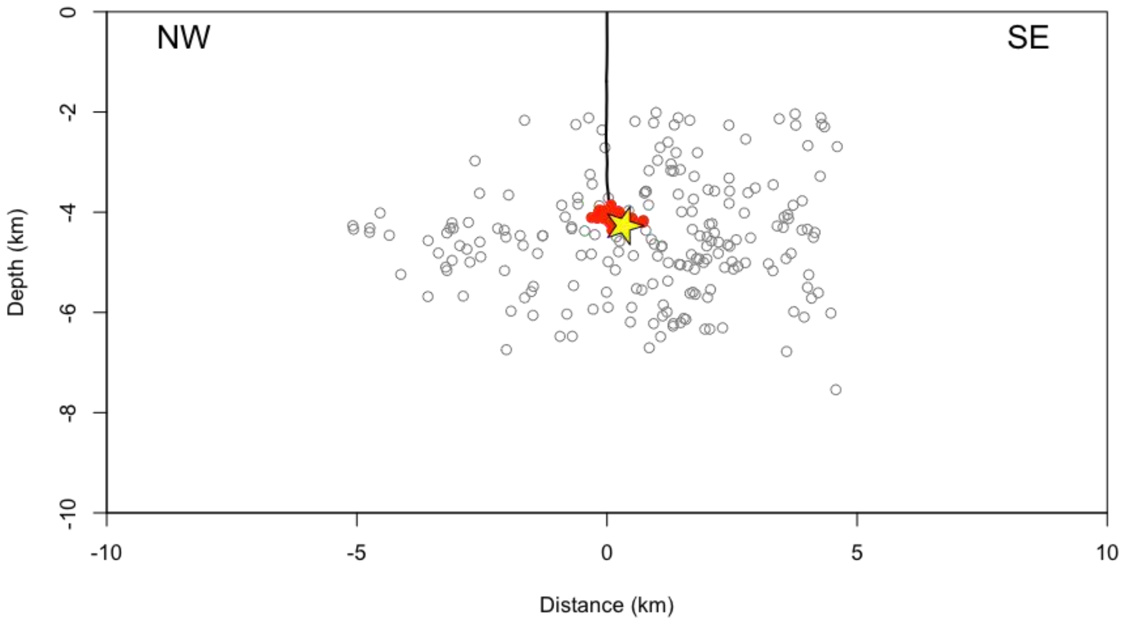

Figure 8. Longitudinal cross section along the Pohang earthquake fault plane showing aftershocks recorded on the day following the M_W 5.5 earthquake (November 16, 2017; gray circles). PX-2 well shown by black line. Hypocenters of earthquakes stimulated by injection into PX-2 in red; mainshock yellow star.

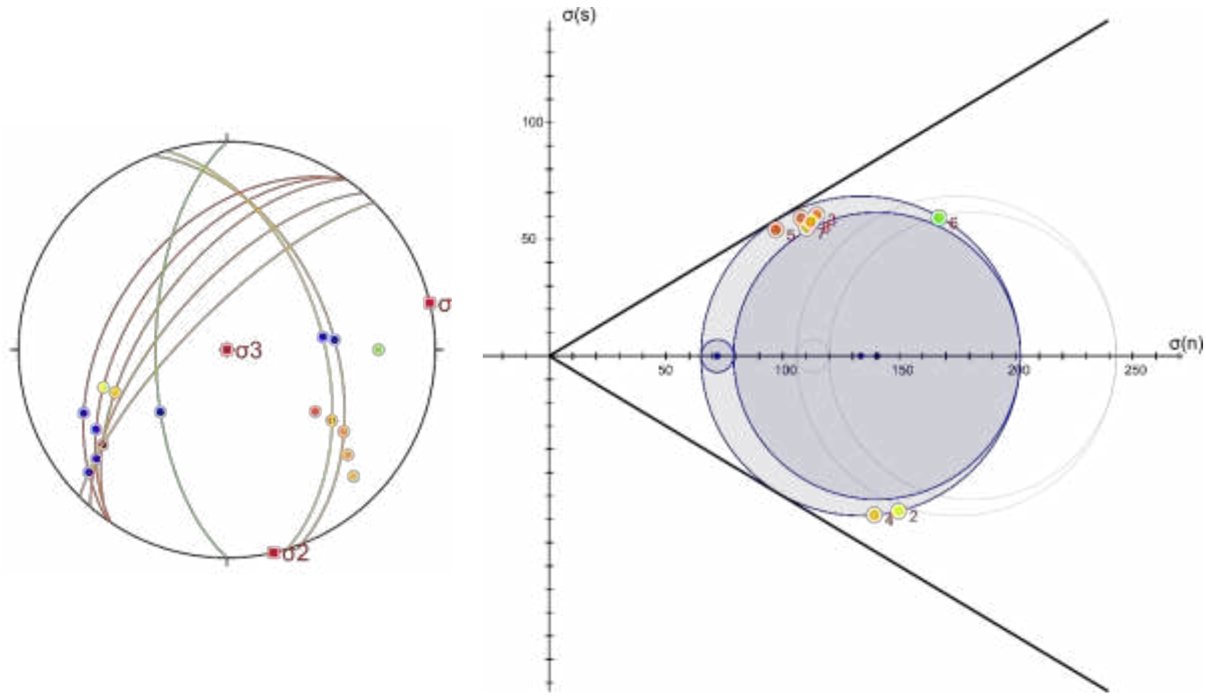

Figure 9. (Left) Stereonet showing the orientations of planes of interest and the corresponding normal vectors, numbered as described in the text and colored according to proximity to slip; red denotes planes closest to failure and green denotes planes furthest from failure. Blue dots mark the calculated shear vectors on each plane. (Right) Mohr diagram calculated for the preferred stress model and a hydrostatic fluid pressure at a depth of 4.2 km. The black diagonal lines demarcate the stresses required for frictional reshear of a cohesionless plane with a friction coefficient of 0.6. The dots are colored according to the proximity of each plane to frictional failure as in the left-hand image. σ(s) and σ(n) denote shear and normal stress, respectively.

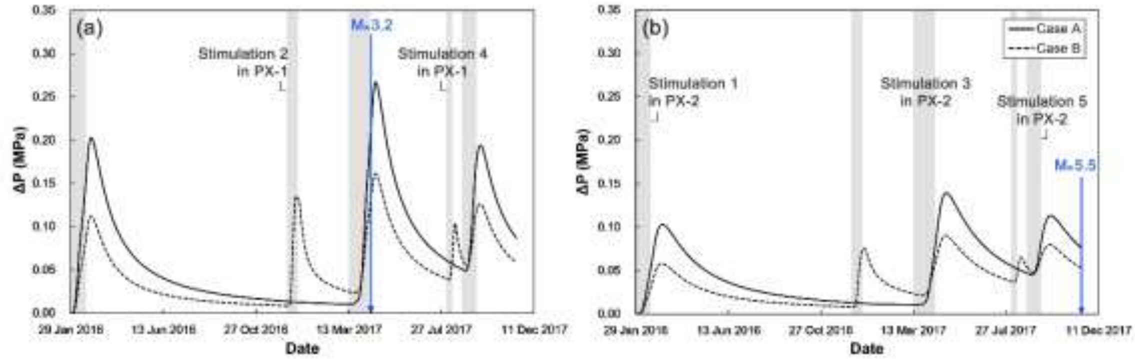

Figure 10. Pore pressure change with time at the M_W 3.2 (a) and M_W 5.5 (b) hypocenters.

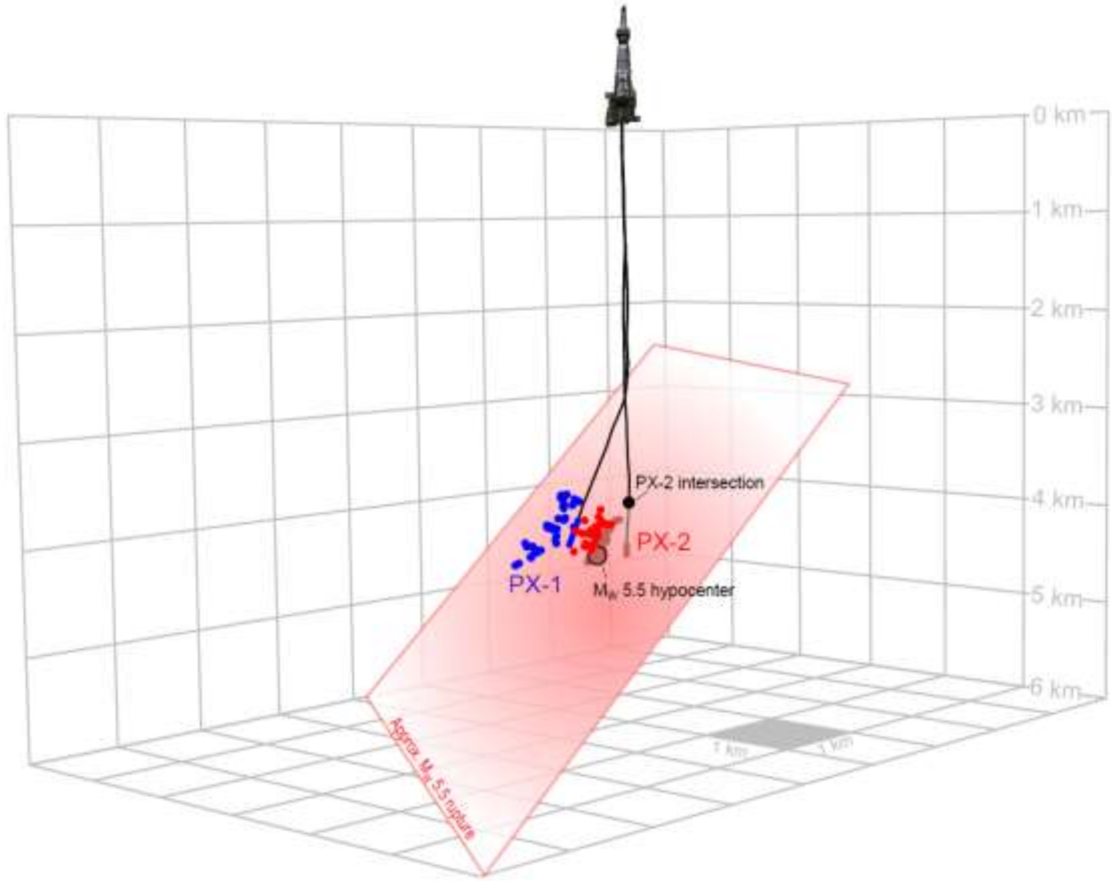

Figure 11. Schematic illustration of the sequence of seismicity associated with stimulation of PX-1 and PX-2, and the relationship of the seismicity to the rupture plane of the M_W 5.5. Pohang earthquake. The view is towards the northeast. The gray grid has 1 km spacing and extends from the surface to 6 km depth. The mainshock fault plane extends from 2.5 km to 6 km and intersects the PX-2 well at 3.8 km. Open hole section of PX-1 and associated seismicity shown in blue sits above and in the hanging wall of the fault plane. The fault plane cuts the seismicity associated with PX-2, shown in red.